Supporting Information

# Optical gap-surface plasmon metasurfaces for spin-controlled surface plasmon excitation and anomalous beam steering

*Chao Meng,*[†] *Shiwei Tang,* [†,‡] *Fei Ding,**[,†] *and Sergey I. Bozhevolnyi**[,†]

[†]Centre for Nano Optics, University of Southern Denmark, Campusvej 55, DK-5230 Odense, Denmark

[‡]School of Physical Science and Technology, Ningbo University, Ningbo, 315211, China

***Corresponding to:** feid@mci.sdu.dk, seib@mci.sdu.dk

**This PDF file includes:**

Number of pages: 11.

Number of figures: 11.

## 1. Beam-position-dependent SPP coupling efficiency under focused RCP incident light

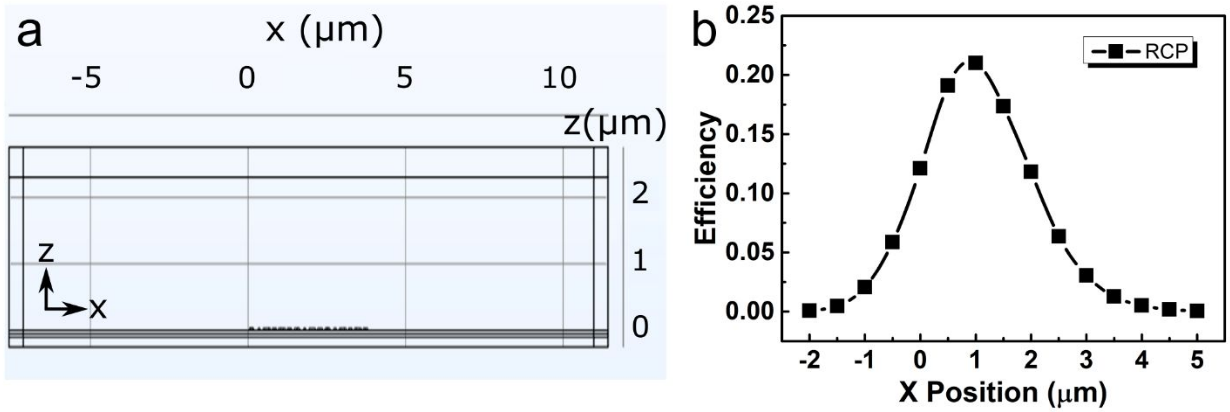


**Figure S1**. (a) Simulation model for evaluating SPP coupling efficiency. The first nanoparticles on the top-layer of the metasurface is centered at $(x_0, y_0, z_0) = (\Lambda/2, 0, t_m/2) = (0.12, 0, 0.175)$ $\mu$m. (b) Calculated beam-position-dependent SPP coupling efficiency of the left-propagating SPPs under focused RCP incident light (beam radius ~ 1 $\mu$m) at 850-nm-wavelength.

## 2. Experimental Setup

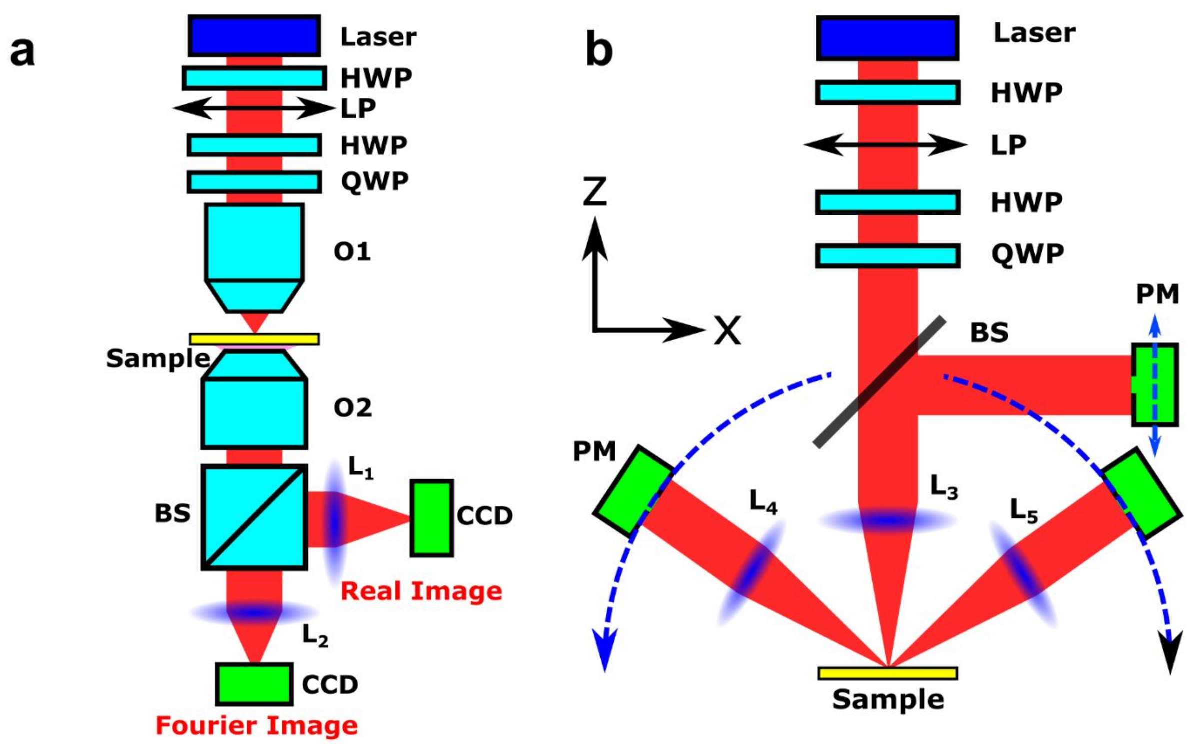

**Figure S2**. (a) Leakage radiation microscopy. (b) Optical setup for measuring the diffraction efficiencies and farfield reflection patterns of the metasurface. Laser: Spectra Physics 3900S Ti: Sapphire laser, HWP: half-wave plate, LP: linear polarizer, QWP: quarter-wave plate, $O_1$: focusing objective (magnification 60×, numerical aperture $NA$ = 0.85), $O_2$: oil-immersion objective (63×, $NA$ = 1.25), BS: beam splitter, $L_1$: convex lens ($f$ = 50 mm), $L_2$: tube lens ($f$ = 200 mm), $L_3$~$L_5$: convex lens ($f$ = 50 mm), PM: optical power meter.

### 3. Experimental characterization of the unidirectional SPP coupling under RCP incidence

### 3.1 SPP propagation lengths

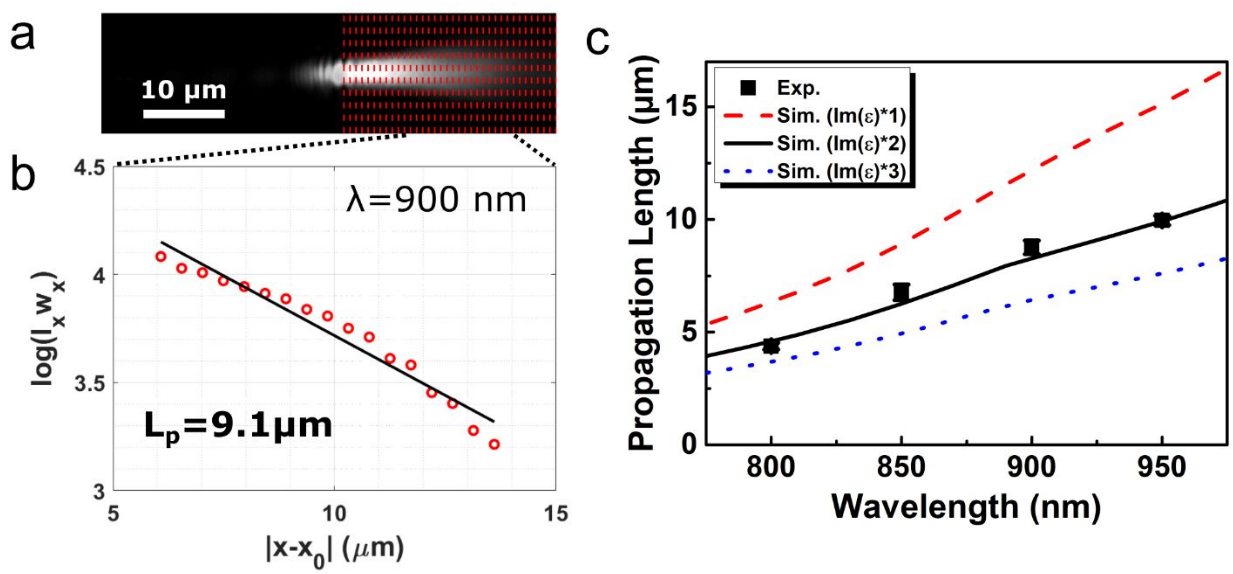


**Figure S3**. (a) LRM image of the propagating SPPs excited by RCP light at 900-nm-wavelength. (b) Variation of the multiplication of SPP intensity and beam waist ($I_x w_x$) on a logarithmic scale as a function of the distance $|x-x_0|$, where $x_0$ is the beam spot center of the incident light. The first order polynomial fitted to the data points (black line) is used to evaluate the propagation length. (c) Experimental (black dots) and calculated (red, black and blue lines) wavelength-dependent propagation lengths. Three calculated results are obtained by adding 3 different weight factors to the imaginary part of the Au's permittivity.

### 3.2 Effective mode index of SPP mode with finite and infinite bottom gold layer

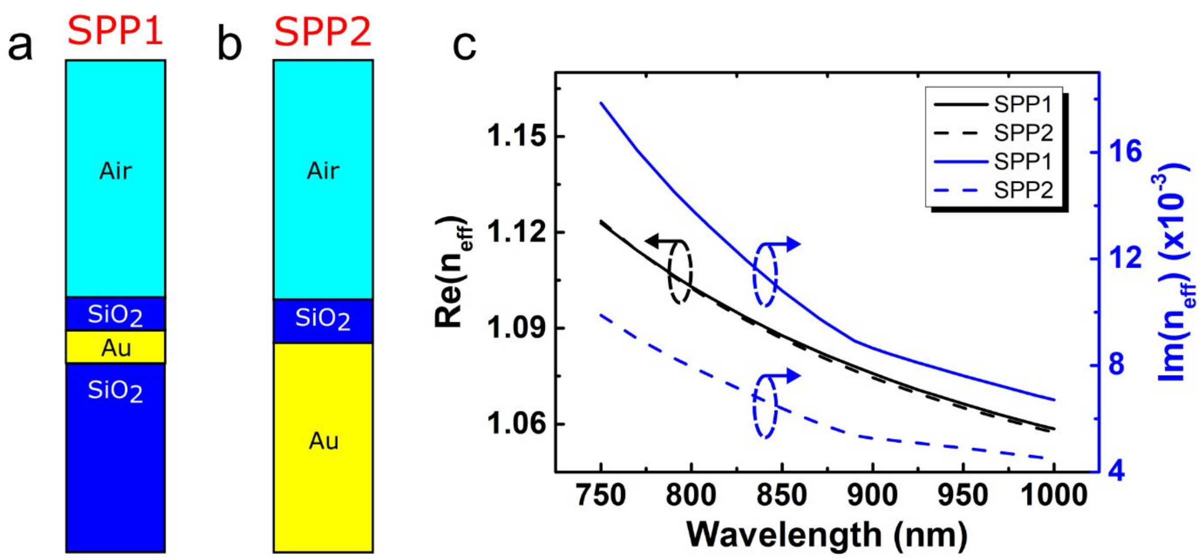


**Figure S4**. Cross section of the SPP waveguide with (a) finite (50-nm-thickness, SPP1, with leakage loss) and (b) infinite (SPP2, without leakage loss) bottom gold layer. (c) Wavelength-dependent effective mode indices of SPP1 and SPP2.

### 3.3 Simulated unidirectional SPP coupling under RCP incident light at λ = 850 nm

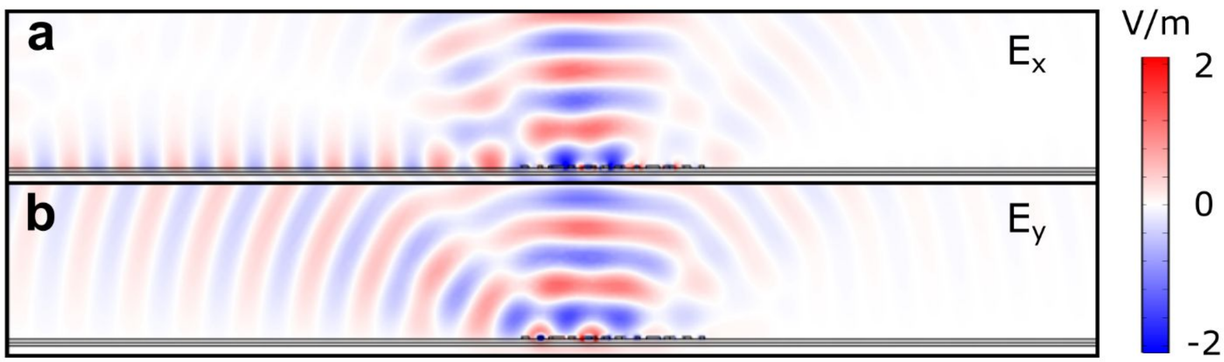


**Figure S5.** Calculated (a) E$x$ and (b) E$y$ components corresponding to SPP coupling under normally incident RCP Gaussian beam ($w_0 = 1\ \mu m$).

### 3.4 LRM characterization of unidirectional SPP coupling by spin-decoupled GSP gradient metasurface under RCP incident light at different wavelengths.

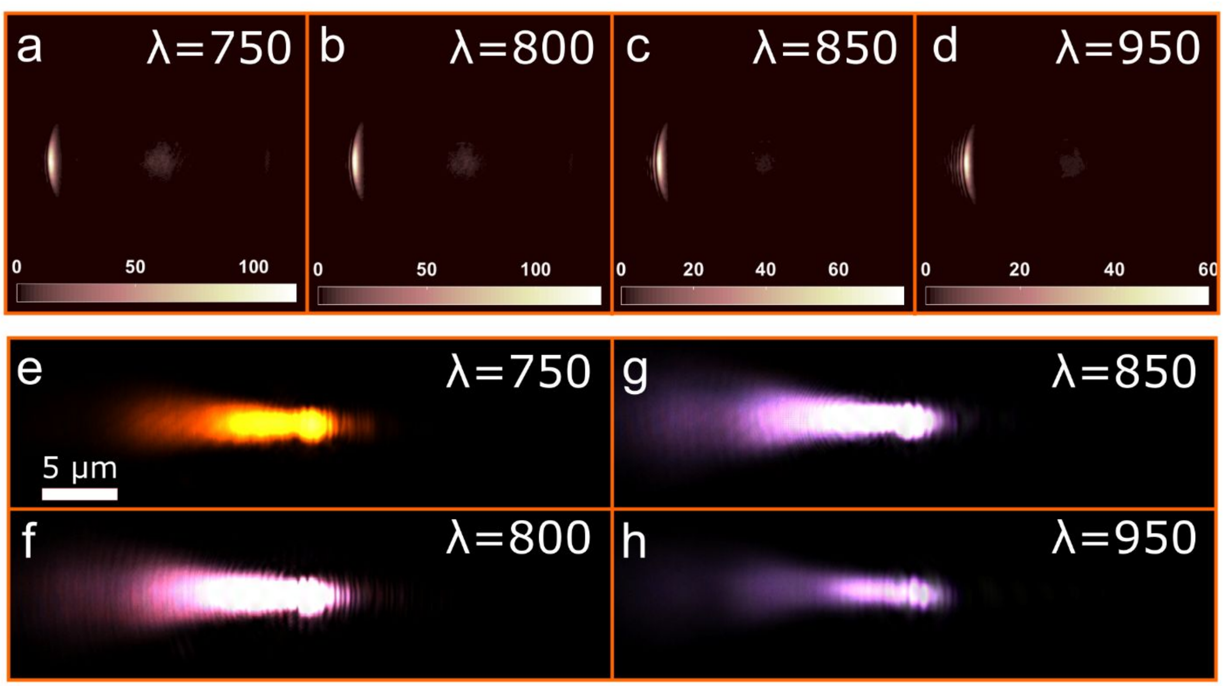


**Figure S6**. (a-d) Fourier and (e-h) LRM images of unidirectional SPP excitation under RCP incident light at 750-nm, 800-nm, 850-nm and 950-nm-wavelengths. Scale bar in (e) also applies to (g-h).

**3.5 Verification of the phase gradient by illuminating LCP and RCP light on the left and right edges of the metasurface.**

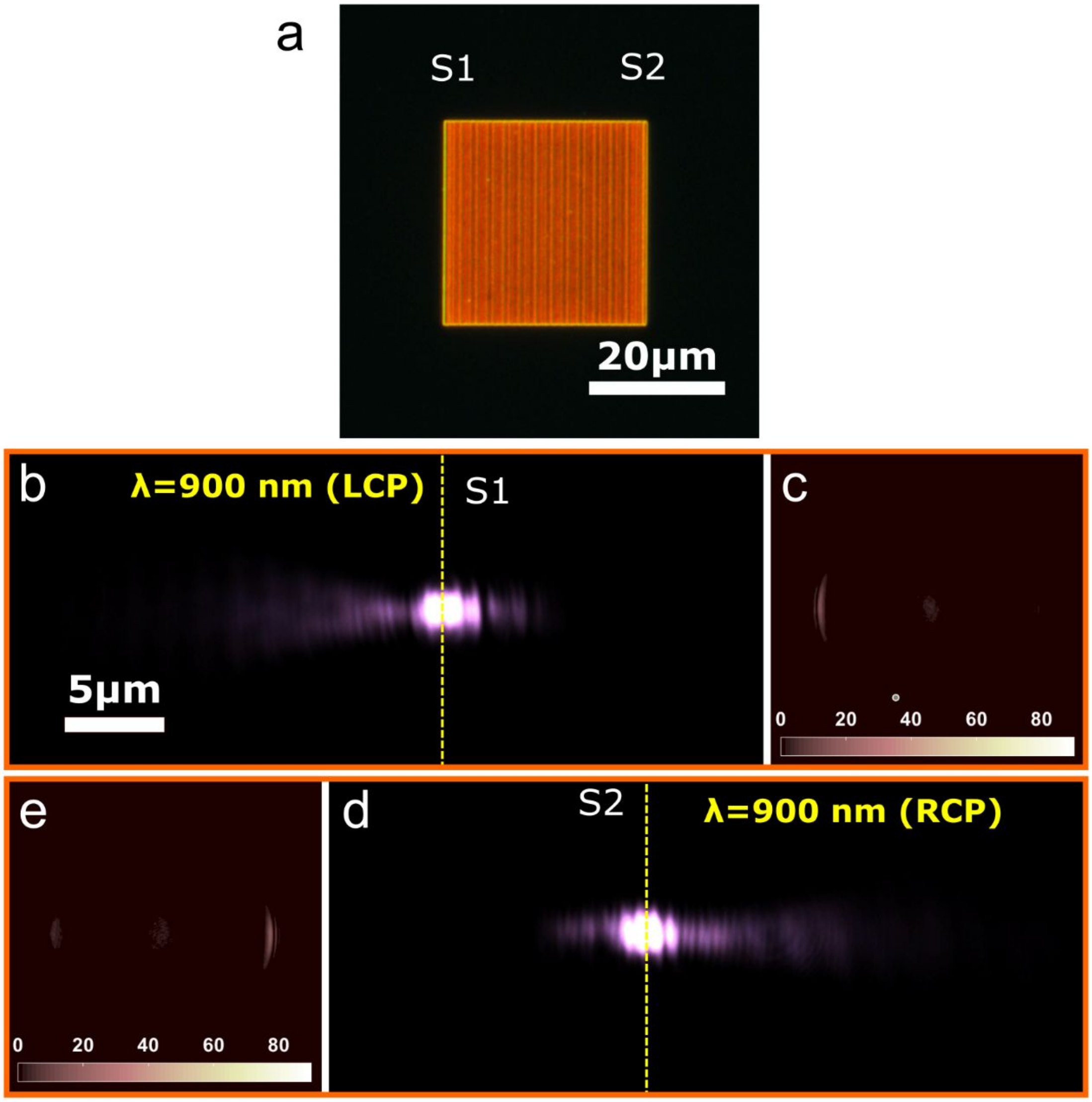


**Figure S7**. (a) Optical microscopic image of the spin-decoupled GSP gradient metasurface, where S1 and S2 indicate the left and right edges of the metasurface along $x$ direction. (b) The LRM and (c) Fourier images under LCP incident light at 900-nm-wavelength. (d) The LRM and (e) Fourier images under RCP incident light at 900-nm-wavelength. Note that the scale bar in (b) also applies to (d).

**4. Calculated reflection fields and farfield patterns from spin-decoupled GSP gradient metasurface under LCP incident light at different wavelengths.**

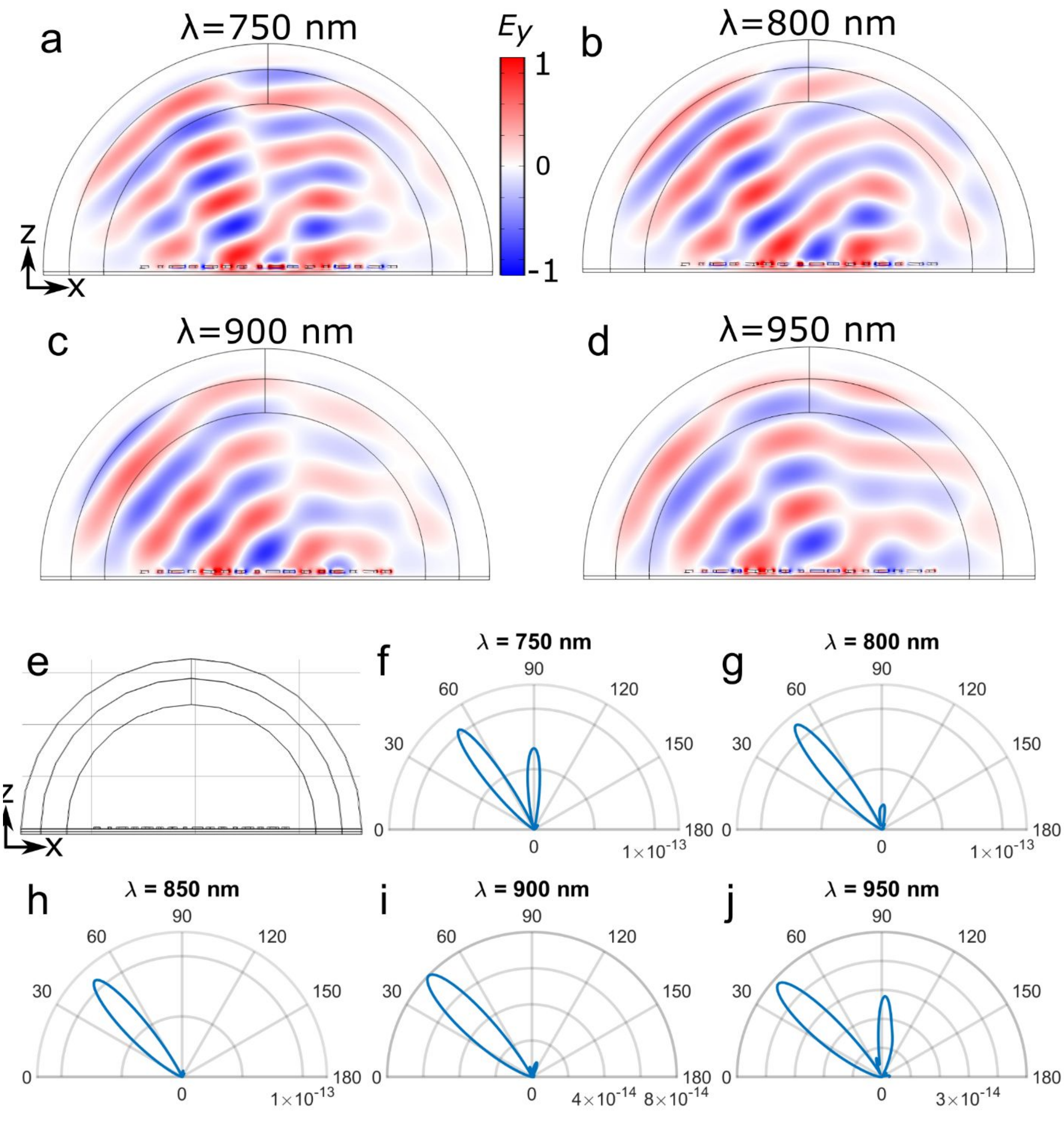


**Figure S8**. (a-d) Calculated electric field (*y*-component) reflected from the metasurface under LCP incident light at 750-nm, 800-nm, 850-nm and 900-nm-wavelengths. (e) Simulation model for calculating farfield reflection patterns and diffraction efficiencies of the spin-decoupled GSP gradient metasurface. (f-j) Calculated farfield reflection patterns from the metasurface under LCP incident light at 750-nm, 800-nm, 850-nm, 900-nm and 950-nm-wavelengths.

## 5. Optical GSP metasurfaces for spin-controlled beam steering and SPP coupling with other propagation/geometric-phase-step pairs ($\Delta\varphi$, $2\Delta\theta$)

First, we define the effective phase period ($P_{\mathrm{eff}}$) of the phase gradients under LCP/RCP incident light:

$$P_{\mathrm{eff}} = 2\pi \Big/ \frac{\partial \varphi_{LCP/RCP}}{\partial x} \tag{1}$$

where $\frac{\partial \varphi_{LCP/RCP}}{\partial x}$ is the reflection phase gradient for the LCP(RCP) incident light. Therefore, the metasurface in the main text has effective phase periods $P_{\mathrm{eff}}(\mathrm{LCP}) = -5.1843\Lambda$ and $P_{\mathrm{eff}}(\mathrm{RCP}) = -3.2562\Lambda$ (phase profiles shown in Fig. 3c), respectively, equivalent to 5.1843 and 3.2562 elements in one phase period for LCP and RCP incident light. Here, by using the effective phase period concept, we could visualize the phase sampling intuitively, and calculate corresponding diffraction angles easily. For example, the metasurface in the main text acts as anomalous beam deflector [reflection angle: $\mathrm{asin}\left(\frac{\lambda}{5.1843\Lambda}\right) \approx 43.1°$] and unidirectional SPP coupler [$3.2562\Lambda = \lambda_{\mathrm{SPP}}$] for LCP and RCP incident light, respectively.

According to the sampling theory, the more elements involved, the higher efficiency can be achieved. Here, by changing the number of HWPs $N_{\mathrm{elem}}$, we could change the effective phase periods to improve the efficiency to some extent. But it will have different effects on the two functionalities since the effective phase periods are distinctly depending on the $N_{\mathrm{elem}}$. In our design, $P_{\mathrm{eff}}(\mathrm{RCP})$ should be maintained constant with different $N_{\mathrm{elem}}$ to satisfy the phasematching condition for the SPP excitation ($\frac{d\varphi_{RCP}}{dx} = k_0 N_{\mathrm{eff}}$). On the other hand, $P_{\mathrm{eff}}$(LCP) changes in a non-monotonic way with $N_{\mathrm{elem}}$, corresponding to different diffraction directions.

If $N_{\mathrm{elem}}$ is increased to 6 in a new metasurface design utilizing, for example, cross-shaped GSP meta-atoms, $P_{\mathrm{eff}}$(RCP) keeps the same value, -3.2562$\Lambda$, to guarantee efficient SPP coupling, while $P_{\mathrm{eff}}$(LCP) changes accordingly to another period, -37.4164$\Lambda$, resulting in 3.2562 and 37.4164 elements in one phase period for the LCP and RCP incident light. Importantly, the beam steering and SPP coupling efficiencies under the LCP and RCP incident light are expected, according to our simulations, to increase by ~10% and ~4%, respectively. Note that in these new simulations, we also increase the imaginary part of gold permittivity by a factor of 2, to be consistent with the simulations in the main text. As a final comment, it should be mentioned that adding more meta-atoms might become challenging for the design and fabrication, thereby introducing more imperfections and decreasing experimentally obtained efficiencies.

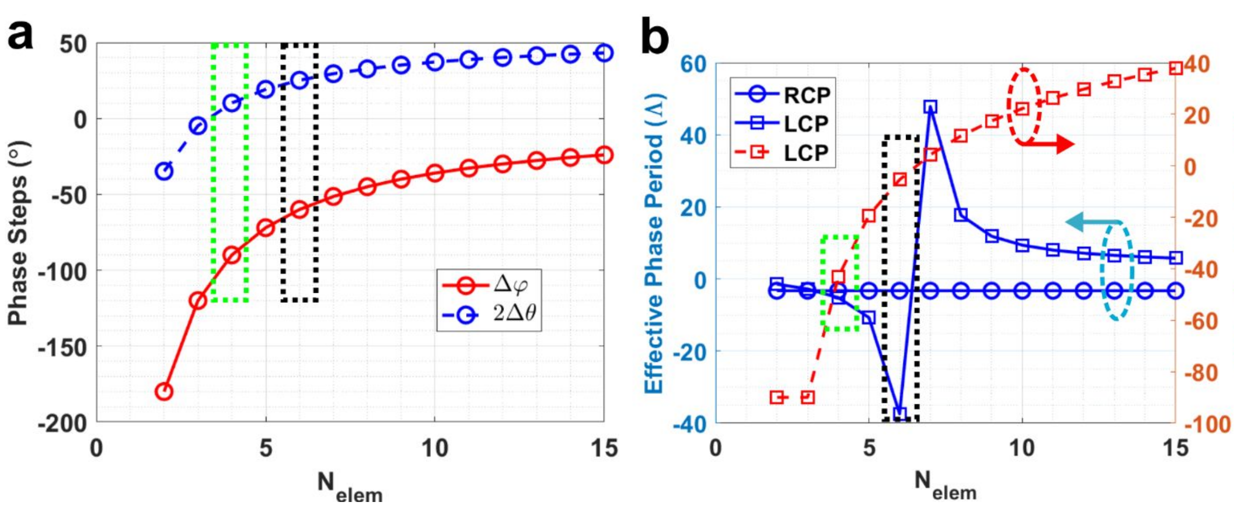


Figure S9. (a) Calculated propagation phases $\Delta\varphi$ (red circles) and geometric phases $2\Delta\theta$ (blue circles) for the spin-decoupled metasurface as a function of the number of meta-atoms $N_{\mathrm{elem}}$. (b) Calculated effective phase periods (LCP: blue squares, RCP: blue circles) and diffraction angles ($\theta$, red squares) of the spin-decoupled metasurface as a function of the number of meta-atoms

$N_{elem}$. Green and black dotted boxes correspond to the metasurface designs with $N_{elem}$ = 4 (main text) and $N_{elem}$ = 6 (Fig. S10), $\Lambda$ = 240 nm.

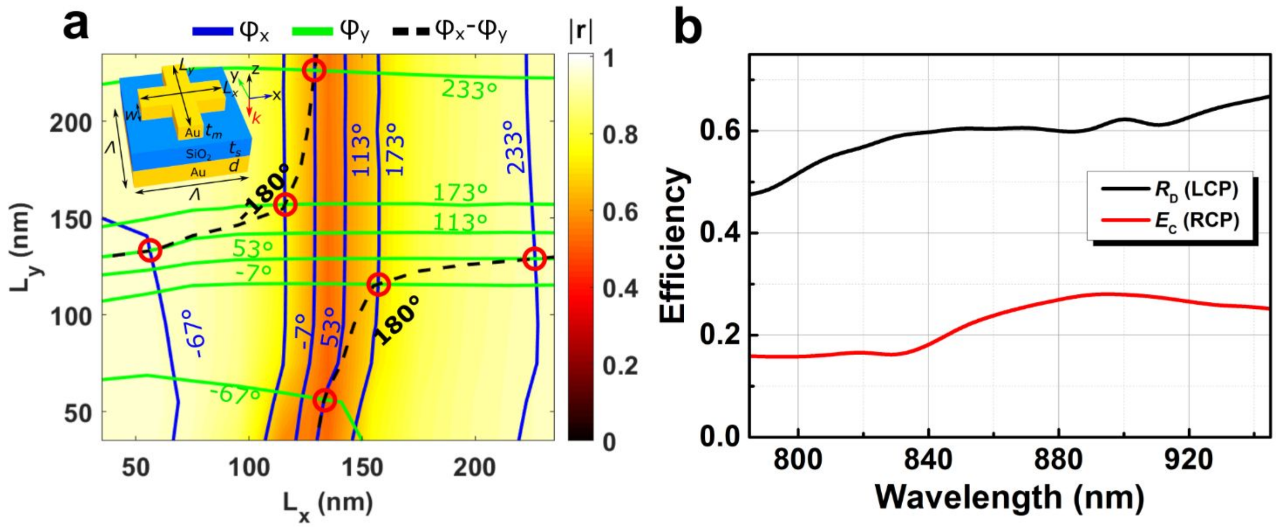


Figure S10. (a) Calculated complex reflection coefficients $r$ as a function of dimensions ($L_x$, $L_y$) of the cross-shaped GSP meta-atoms for $\Lambda$ = 240 nm, $t_m$ = 35 nm, $w$ =50 nm and $d = t_s$ = 50 nm at 850-nm-wavelength. Color maps show the reflection coefficient magnitudes for $x$-polarization, while the blue and green solid lines are contours of the reflection coefficient phases for $x$- and $y$-polarization. Black dashed lines indicate the nano-HWPs with $|\varphi_x-\varphi_y|$ equal to 180°. Inset is the sketch of the cross-shaped GSP meta-atom. (b) Calculated wavelength-dependent beam steering (black line) and SPP coupling (red line) efficiencies under LCP and RCP incident light.

**6. Calculated metasurface efficiencies with different weight factors on the imaginary part of gold permittivity**

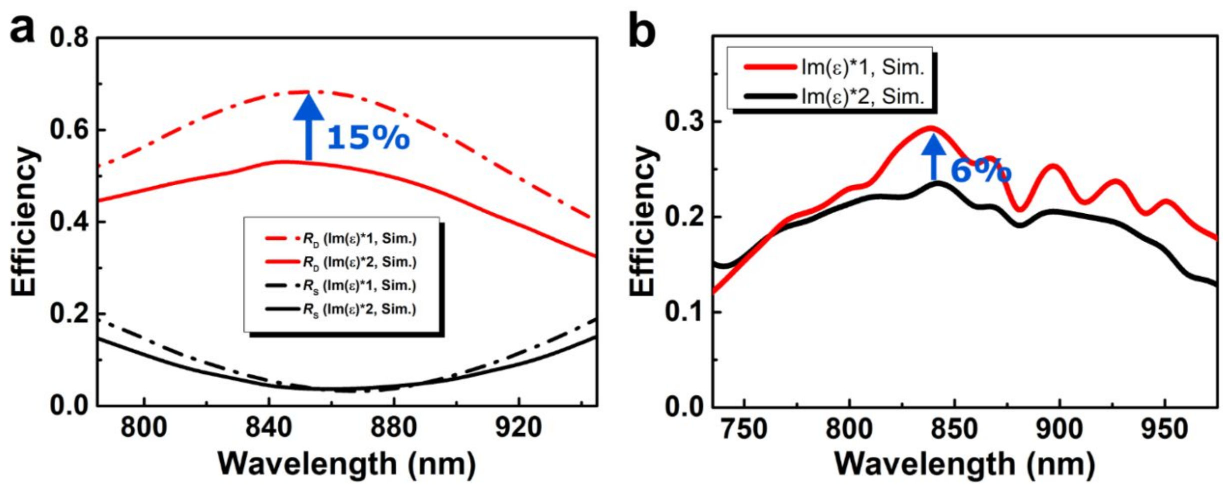


Figure S11. Calculated wavelength-dependent (a) beam steering and (b) SPP coupling efficiencies with different weight factors of the imaginary part of the gold permittivity under LCP and RCP incident light, respectively. Note that the metasurface design is the same as the one in the main text.